

## Chapter 5

### The concept of JEBAR: Evolution of baroclinic planetary eddies over localized bottom topography

#### 5.1 Introduction

A baroclinic current flowing over sloping bottom topography on the rotating solid earth can generate a barotropic flow field by releasing the available potential energy. This concept, that is called JEBAR (joint effect of baroclinicity and relief), has been a powerful tool to explain some fundamental mechanisms in the ocean circulation. As a compact review in the context of the general ocean circulation, one may refer to Sakamoto and Yamagata (1996) (hereafter SY). In the context of climatology and long-term variations, several diagnostic ocean models suggest that JEBAR dominates the gyre-scale ocean circulations in both of the North Atlantic and the North Pacific and that the climatologies of the external wind forcing are of less significance (Greatbatch et al., 1991; Myers et al., 1996; Myers and Weaver, 1996). This is not surprising when considering that the major input of vorticity is originated in the rotating solid earth and that the available potential energy due to large-scale stratification is undoubtedly enormous in those gyres.

On the other hand, JEBAR also plays a crucial role in the seasonal variations in the wind-driven ocean circulation (SY). The available potential energy accumulated by the wind action is continually released over the continental slope to produce a subgyre-scale recirculation. As a result, the seasonal transport variation of the wind-driven gyre is "rectified" compared with the large amplitude of the actual wind variation. The above mechanism was demonstrated in SY using two-layer planetary geostrophic equations as the most canonical model because the model retains the basic factors required to describe the importance of JEBAR in the large-scale ocean circulation; i.e., baroclinic long Rossby waves and varying bottom topography (Salmon, 1992).

Furthermore, the recent TOPEX/POSEIDON satellite altimeter data (Chelton and Schlax, 1996) show that oceanic baroclinic Rossby waves observed in the extratropical Pacific have higher phase speeds than those predicted by the standard linear theory. Chelton and Schlax (1996) suggest that those Rossby waves may be distorted and

amplified by bottom topography. Eddy trajectories detected by neutrally buoyant floats in the Sargasso Sea (Freeland et al., 1975) also imply topographic control.

The above results from the models and the observations motivate us to demonstrate the basic properties of JEBAR both on planetary geostrophic and on quasigeostrophic scales in a manner of geophysical fluid dynamics. In this paper, we solve numerically the two-mode equations with weak dissipation and with no external forcing [see (5.31) and (5.32)] as an initial value problem of a Gaussian-type, pure baroclinic eddy interacting with a specified meridional ridge (or trench). This particular choice of topography is due to ubiquity in the real ocean as well as mathematical simplicity. In this way, we describe the effect of localized bottom topography on pure baroclinic eddies in terms of JEBAR.

With regard to the present problem, Barnier (1988) introduced an ocean ridge as a generator of Rossby waves of annual period. Using a two-layer quasigeostrophic model with realistic seasonal winds, he found that a baroclinic Rossby wave excited at an eastern boundary is attenuated above the ridge by releasing its potential energy to build up a barotropic mode; a wind-forced barotropic mode, on the other hand, may cause discontinuity over the ridge, leading to a baroclinic mode. Louis and Smith (1982) discussed the radiation of a barotropic field by a barotropic eddy over a topographic slope. The motion of a barotropic eddy over sloping bottom topography is investigated by several authors (e.g., Grimshaw et al., 1994a). We also count only a few studies on a baroclinic eddy in the presence of bottom topography. Henrotay (1981) analyzed continuously stratified, quasigeostrophic equations and showed that the coupled effect of a mean flow and bottom topography may affect the amplitude and phase speed of a solitary baroclinic eddy. Smith and O'Brien (1983) and Smith (1986) used two-layer primitive equations and concluded that the combination of topographic waves and nonlinear self-advection determines the direction of the eddy motion.

In the numerical experiments with a flat bottom, quasigeostrophic mesoscale eddies with strong nonlinearity show some interesting features such as meridional migration and baroclinic instability (e.g., McWilliams and Flierl, 1979). The planetary geostrophic eddies may possess the strong nonlinearity due to large horizontal divergence, and hence, despite the lack of the relative vorticity, may exhibit similar tendencies due to JEBAR.

Our plan of this chapter is as follows. In Section 5.2, the planetary geostrophic equations are derived from the two-layer primitive equations. The model ocean, initial conditions and parameters used in the experiments are given in Section 5.3. Section 5.4 presents the numerical results of the planetary geostrophic eddies and discusses the westward motion of the baroclinic field and the barotropic flow field generated by energy conversion. We particularly focus on the role of JEBAR in this section. In Section 5.5, some complementary experiments using similar equations but appropriate

to smaller scale (say 100–200 km) eddies are presented. Section 5.6 is assigned to summary and discussion.

## 5.2 Formulation

In this section, we derive a set of governing equations in two-mode form appropriate to planetary-scale motions. This is because JEBAR is intrinsically barotropic-baroclinic interaction through topography. We also derive subset of similar equations but for smaller-scale motions for later use in order to examine JEBAR in quasigeostrophic motions. We start with two-layer primitive equations on a  $\beta$ -plane including Rayleigh damping and bottom topography. Integrating vertically within each layer (denoted by subscripts 1 and 2) and introducing rigid-lid, hydrostatic and Boussinesq approximations, those equations are

$$U_{1t} + \left(\frac{1}{h_1}U_1U_1\right)_x + \left(\frac{1}{h_1}V_1U_1\right)_y - fV_1 = -\frac{1}{\rho_0}h_1p_x - rU_1, \quad (5.1)$$

$$V_{1t} + \left(\frac{1}{h_1}U_1V_1\right)_x + \left(\frac{1}{h_1}V_1V_1\right)_y + fU_1 = -\frac{1}{\rho_0}h_1p_y - rV_1, \quad (5.2)$$

$$h_{1t} + U_{1x} + V_{1y} = 0, \quad (5.3)$$

$$U_{2t} + \left(\frac{1}{h_2}U_2U_2\right)_x + \left(\frac{1}{h_2}V_2U_2\right)_y - fV_2 = -\frac{1}{\rho_0}h_2p_x + g'h_2h_{1x} - rU_2, \quad (5.4)$$

$$V_{2t} + \left(\frac{1}{h_2}U_2V_2\right)_x + \left(\frac{1}{h_2}V_2V_2\right)_y + fU_2 = -\frac{1}{\rho_0}h_2p_y + g'h_2h_{1y} - rV_2, \quad (5.5)$$

$$h_{2t} + U_{2x} + V_{2y} = 0, \quad (5.6)$$

where  $(U_n, V_n) = (h_n u_n, h_n v_n)$  ( $n = 1, 2$ ) are the horizontal components of volume transport of each layer;  $(u_n, v_n)$  are the components of horizontal velocity and  $h_n$  is the  $n$ th-layer thickness defined by

$$h_1 = D_1 - \eta \quad \text{and} \quad h_2 = D_2 + \eta - h_B, \quad (5.7)$$

where  $D_n$  are the constant layer depth,  $\eta$  is the displacement of the interface and  $h_B$  is the bottom topography. The other notations are conventional: the Coriolis parameter  $f = f_0 + \beta_0 y$ , the depth-independent pressure  $p(x, y)$ , the mean density  $\rho_0$  and the reduced gravity  $g' = (\rho_2 - \rho_1)/\rho_0$ . The Rayleigh damping coefficient is denoted by  $r$ .

Using the characteristic length scale  $L$ , velocity scale  $u_0$  and depth scale  $D = (D_1 + D_2)$ , we nondimensionalize variables as follows:

$$(U_n, V_n) = L(x, y), \quad (U_n, V_n) = u_0 D(U_n, V_n), \quad p = \rho_0 f_0 u_0 L p_*, \\ h_n = D h_{n*}, \quad \eta = \frac{f_0 u_0 L}{g'} \frac{D}{D_2} \eta_*, \quad h_B = D h_{B*}$$

and

$$\begin{aligned} t &= (L/\bar{c})t_* & \text{for the momentum equations,} \\ t &= (L/\hat{c})t_* & \text{for the continuity equations,} \end{aligned}$$

(dimensionless variables are denoted temporarily by an asterisk) where

$$\bar{c} \equiv \beta_0 \bar{L}_D^2 \equiv \beta_0 \frac{gD}{f_0^2} \quad \text{and} \quad \hat{c} \equiv \beta_0 \hat{L}_D^2 \equiv \beta_0 \frac{g'D_1 D_2}{f_0^2 D} \quad (5.8)$$

are the phase speeds of long barotropic and baroclinic Rossby waves, respectively. New length scales  $\bar{L}_D$  and  $\hat{L}_D$  denote the barotropic Rossby radius and baroclinic Rossby radius, respectively. With the above scaling, we have the nondimensionalized equations:

$$\frac{\beta}{\bar{F}} U_{1t} + Ro \left[ \left( \frac{1}{\bar{h}_1} U_1 U_1 \right)_x + \left( \frac{1}{\bar{h}_1} V_1 U_1 \right)_y \right] - fV_1 = -h_1 p_x - kU_1, \quad (5.9)$$

$$\frac{\beta}{\bar{F}} V_{1t} + Ro \left[ \left( \frac{1}{\bar{h}_1} U_1 V_1 \right)_x + \left( \frac{1}{\bar{h}_1} V_1 V_1 \right)_y \right] + fU_1 = -h_1 p_y - kV_1, \quad (5.10)$$

$$\frac{\beta}{\bar{F}} h_{1t} + Ro(U_{1x} + V_{1y}) = 0, \quad (5.11)$$

$$\frac{\beta}{\bar{F}} U_{2t} + Ro \left[ \left( \frac{1}{\bar{h}_2} U_2 U_2 \right)_x + \left( \frac{1}{\bar{h}_2} V_2 U_2 \right)_y \right] - fV_2 = -h_2 p_x + \frac{1}{Ro\hat{F}d_1 d_2} h_2 h_{1x} - kU_2, \quad (5.12)$$

$$\frac{\beta}{\bar{F}} V_{2t} + Ro \left[ \left( \frac{1}{\bar{h}_2} U_2 V_2 \right)_x + \left( \frac{1}{\bar{h}_2} V_2 V_2 \right)_y \right] + fU_2 = -h_2 p_y + \frac{1}{Ro\hat{F}d_1 d_2} h_2 h_{1y} - kV_2, \quad (5.13)$$

$$\frac{\beta}{\bar{F}} h_{2t} + Ro(U_{2x} + V_{2y}) = 0, \quad (5.14)$$

and

$$h_1 = d_1 - Ro\hat{F}d_1\eta \quad \text{and} \quad h_2 = d_2 + Ro\hat{F}d_1\eta - \alpha h_B, \quad (5.15)$$

where  $\alpha \equiv L/L_B$  with  $L_B$  another length scale for the bottom topography. The nondimensional parameters are defined by

$$\beta = \frac{\beta_0 L}{f_0}, \quad \bar{F} = \frac{f_0^2 L^2}{gD} = \left( \frac{L}{\bar{L}_D} \right)^2, \quad \hat{F} = \frac{f_0^2 L^2 D}{g'D_1 D_2} = \left( \frac{L}{\hat{L}_D} \right)^2$$

(note that  $\beta/\bar{F} = \bar{c}/(f_0 L)$  and so forth), and

$$Ro = \frac{u_0}{f_0 L}, \quad d_n = \frac{D_n}{D}, \quad k = \frac{r}{f_0}.$$

### 5.2.1 The planetary geostrophic equations

We first consider the following parameter regime (cf. Williams and Yamagata, 1984):

$$\beta \rightarrow 1, \quad Ro \ll 1, \quad Ro\hat{F} \rightarrow 1, \quad \alpha \rightarrow 1. \quad (5.16)$$

Furthermore, we hereafter treat the extreme case of a barotropic Rossby wave with infinite  $\bar{c}$  just for simplicity, so that the barotropic adjustment takes place instantaneously. Then, the horizontal velocity depends on time  $t$  only parametrically. The main balance is reduced to

$$-fV_1 = -h_1 p_x - kU_1, \quad (5.17)$$

$$fU_1 = -h_1 p_y - kV_1, \quad (5.18)$$

$$\beta h_{1t} + \delta(U_{1x} + V_{1y}) = 0, \quad (5.19)$$

$$-fV_2 = -h_2 p_x + \frac{1}{d_1 d_2 \delta} h_2 h_{1x} - kU_2, \quad (5.20)$$

$$fU_2 = -h_2 p_y + \frac{1}{d_1 d_2 \delta} h_2 h_{1y} - kV_2, \quad (5.21)$$

$$\beta h_{2t} + \delta(U_{2x} + V_{2y}) = 0, \quad (5.22)$$

with

$$h_1 = d_1 - d_1 \delta \eta \quad \text{and} \quad h_2 = d_2 + d_1 \delta \eta - h_B, \quad (5.23)$$

where

$$\delta = \frac{\Delta_1}{D_1} \quad (5.24)$$

measures the initial amplitude of the interface displacement,  $\Delta_1$ , relative to the undisturbed upper-layer depth. That is, the advective velocity scale  $u_0$  is related to  $\Delta_1$  by geostrophic balance in the upper layer:

$$u_0 = \frac{g'\Delta_1 D_2}{f_0 L D}. \quad (5.25)$$

In this particular regime,  $\delta \rightarrow 1$  [see (5.16)] as usual for planetary ocean eddies. From (5.19) and (5.22), the transport streamfunction  $\psi$  is defined by

$$U_1 + U_2 = -\psi_y \quad \text{and} \quad V_1 + V_2 = \psi_x. \quad (5.26)$$

On the other hand, from (5.17), (5.18), (5.20), (5.21) and using (5.26), we have

$$U_1 = -\frac{h_1}{H} \psi_y + \frac{1}{d_1 d_2 \delta} \frac{h_1 h_2}{f^2 H} (-fh_{1y} - kh_{1x}), \quad (5.27)$$

$$V_1 = \frac{h_1}{H} \psi_x + \frac{1}{d_1 d_2 \delta} \frac{h_1 h_2}{f^2 H} (+fh_{1x} - kh_{1y}), \quad (5.28)$$

$$U_2 = -\frac{h_2}{H} \psi_y - \frac{1}{d_1 d_2 \delta} \frac{h_1 h_2}{f^2 H} (-fh_{1y} - kh_{1x}), \quad (5.29)$$

$$V_2 = \frac{h_2}{H} \psi_x - \frac{1}{d_1 d_2 \delta} \frac{h_1 h_2}{f^2 H} (+fh_{1x} - kh_{1y}), \quad (5.30)$$

where  $H = h_1 + h_2$  is the total depth and we have neglected  $k^2$  compared with  $f^2$ .

Adding lower-layer equations [(5.20), (5.21)] to the upper-layer equations [(5.17), (5.18)] and taking the curl after dividing by  $H$ , we obtain the barotropic potential vorticity equation:

$$J\left(\psi, \frac{f}{H}\right) = \frac{1}{d_1 d_2 \delta} J\left(\frac{h^2}{2}, \frac{1}{H}\right) - k \nabla \cdot \left(\frac{1}{H} \nabla \psi\right), \quad (5.31)$$

where  $J$  denotes the Jacobian operator and  $h_1$  is replaced by  $h$  for simplicity. We prefer  $h$  to  $\eta$  because  $h$  suffers from  $O(1)$  variations. On the other hand, the continuity equation (5.19) yields the baroclinic equation which governs the time evolution of the  $h$ -field:

$$\beta h_t + \delta J\left(\psi, \frac{h}{H}\right) + J\left(h, \frac{h(H-h)}{f H d_1 d_2}\right) - k \nabla \cdot \left(\frac{h(H-h)}{f^2 H d_1 d_2} \nabla h\right) = 0. \quad (5.32)$$

We note here that the barotropic adjustment is completed instantaneously in the present model by the diagnostic equation (5.31). The baroclinic process, however, is described by the prognostic equation (5.32). We also note that both vertical modes are connected by the JEBAR term [the first term on the right-hand side of (5.31)] and the modal interaction term [the second term of (5.32)]. Salmon (1992) investigated similar equations analytically in relation to the Gulf Stream separation.

### 5.2.2 The quasigeostrophic equations

We next consider the following parameter regime: for  $\epsilon \ll 1$ ,

$$\beta = B\epsilon, \quad Ro = E\epsilon^2, \quad \hat{F} = \frac{F}{E\epsilon}, \quad \alpha h_B = \epsilon \eta_B, \quad (5.33)$$

where  $B$ ,  $E$  and  $F$  are  $O(1)$  marker parameters. In addition, the approximation of  $\bar{c} \rightarrow \infty$  is again introduced to focus on JEBAR. Then, all dependent variables are expanded to the asymptotic series in powers of  $\epsilon$  as a usual manner and are substituted into (5.9)–(5.14). This intermediate scaling in the two-layer system including a moving lower layer leads to linear quasigeostrophic equations. From the  $O(\epsilon)$  balance, the two-mode equations corresponding to this scaling are obtained with Rayleigh damping ( $k = K\epsilon$ ):

$$J(\psi, B y + \eta_B) = J(\eta_B, d_1 d_2^{-1} \eta) - K \nabla^2 \psi, \quad (5.34)$$

$$B \eta_t + F J(\psi, \eta) + J(\psi - \eta, B y) + K \nabla^2(\psi - \eta) = 0, \quad (5.35)$$

where  $\psi = d_1 \psi_1 + d_2 \psi_2$  is the total transport streamfunction with  $\psi_n$  the quasigeostrophic streamfunction of the  $n$ th layer and all dependent variables are of leading

order in the corresponding asymptotic series. We use (5.34) and (5.35) to demonstrate the effect of JEBAR in Section 3.5. Barnier (1988) used the frictionless form of (5.34) and (5.35) to explain the generation mechanism of wind-forced baroclinic Rossby waves over an ocean ridge.

### 5.3 The model

In the main experiment using the planetary geostrophic equations, we assume the following dimensional parameters:

$$\begin{aligned} f_0 &= 1 \times 10^{-4} \text{ s}^{-1}, & \beta_0 &= 1.67 \times 10^{-11} \text{ m}^{-1} \text{ s}^{-1} \quad (\text{at } 43.43^\circ \text{N}), \\ L &= 600 \text{ km} \quad (\text{eddy radius}) \\ D &= 4000 \text{ m}, \quad D_1 = 1000 \text{ m}, \quad D_2 = 3000 \text{ m}, \\ g' &= 0.02 \text{ ms}^{-2}. \end{aligned} \quad (5.36)$$

Thus, the phase speed of the baroclinic Rossby wave is  $\hat{c} = 2.5 \times 10^{-2} \text{ ms}^{-1}$ , the baroclinic Rossby radius  $\hat{L}_D = 38.7 \text{ km}$ , the characteristic time scale  $L/\hat{c} = 279$  days and the corresponding nondimensional parameters are  $\beta = 0.1$ ,  $d_1 = 0.25$  and  $d_2 = 0.75$ . For the Rayleigh damping coefficient, we take  $k = 7.5 \times 10^{-4}$ , corresponding to  $r^{-1} = 154$  days; it will turn out that the Rayleigh damping does not provide a true decay rate for the baroclinic motion (Section 5.4). The eddy amplitude  $\delta$  is varied (0.2 or 0.8) in the experiment. The parameter values for the complementary experiment for the smaller-scale motion will be given in Section 5.5.

Our model ocean is a zonal channel ranging  $0 \leq x \leq 16$  and  $-5 \leq y \leq 5$ , which is broad enough to avoid the boundary effect. Solid walls are located at  $y = \pm 5$ , along which the free-slip condition

$$f h_x = k h_y, \quad (5.37)$$

which is derived from (5.28) and (5.30) with  $\psi = 0$ , is imposed. The bottom topography is given by

$$H = 1 \pm 0.15 \text{sech}^2(x - \delta), \quad (5.38)$$

which represents a meridional ridge (minus sign) or a trench (plus sign), having the same  $e$ -folding width as the eddy radius (Fig. 5.1).

The simultaneous equations (5.31) and (5.32) are solved numerically as an initial value problem. The initial state is a Gaussian eddy given by

$$h = d_1 \left\{ 1 \pm \delta \exp[-(x - 12)^2 - y^2] \right\} \quad \text{at } t = 0, \quad (5.39)$$

where the minus (plus) sign corresponds to a cold (warm) eddy (Fig. 5.1). In the present model, the barotropic component  $\psi$  is produced by the interaction between the baroclinic eddy and the bottom topography.

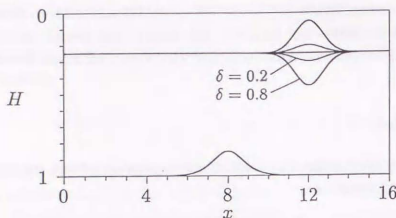


**Figure 5.1.** Vertical section of the zonal channel at  $y = 0$ . Lines plotted are the initial values  $h = 0.25 \{1 - \delta \exp[-(x-12)^2 - y^2]\}$  and the meridional ridge  $H = 1 - 0.15 \operatorname{sech}^2(x-8)$ . The meridional trench (not shown) is just symmetry of the ridge about the flat bottom.

In the actual calculation, the equations are approximated to a centered finite difference form on  $129 \times 81$  regular-spacing grid points with the Arakawa Jacobian (although not necessary for the present nonconservative equations), and are integrated by using the combination of the simple leapfrog and the SOR methods.

## 5.4 JEBAR on the planetary geostrophic motion

### 5.4.1 Overview

In this section, we present the numerical solutions to (5.31) and (5.32). Figures 5.2–5.5 show the time evolution of  $h$  and  $\psi$  for the initial values of moderate amplitude ( $\delta = 0.2$ ). Figure 5.2 (5.3) corresponds to a cold (warm) eddy in the presence of the meridional ridge. Figures 5.4 and 5.5, on the other hand, show solutions for the same eddies in the presence of the trench. In all cases, the baroclinic eddies propagate basically westward at the speed of the long baroclinic planetary wave, but the topography severely deforms the shape and affects the motion of the eddies. Those figures also demonstrate the meridional asymmetry due to the large-scale dynamics. Figure 5.6 shows the zonal motion of the eddy center, which is defined simply by the maximum of the interface displacement, as a function of time. Comparing those diagrams with the field of the streamfunction  $\psi$ , it is easily deduced that the induced barotropic flows may distort properties of the baroclinic eddy. Figure 5.7 shows the geostrophic contours of the lower layer,  $q_2 = f/h_2$ . Finally, energy conversion as a function of time is shown in Fig. 5.8, corresponding to Figs 5.2 and 5.3. Detailed description and explanation of the whole results are presented below.

### 5.4.2 JEBAR forcing and barotropic flow field

We consider here the JEBAR forcing in the barotropic equation (5.31) in the case of a cold eddy impinging on the meridional ridge (Fig. 5.2).

When a cold eddy ascends the eastern flank of the ridge, the JEBAR term generates positive (negative) vorticity at the northern (southern) half of the ridge. This vorticity input allows barotropic currents to cross the  $f/H$  contours; otherwise the currents just follow those contours. When the eddy travels farther westward, a similar argument holds for the western flank of the ridge. Accordingly, a barotropic cyclonic gyre is generated over the ridge together with an anticyclonic gyre just to the south as shown in Fig. 5.2. The JEBAR forcing also emits barotropic waves (with an infinite speed in the present approximation) when the baroclinic eddy interacts with the ridge. The barotropic cyclonic gyre cancels the baroclinic lower-layer anticyclone; this presents a clear example of spontaneous compensation caused by the interaction between the  $h$ -field and the topographic slope. A warm eddy generates a barotropic field of opposite sign (Fig. 5.3). However, the westward barotropic jet over the ridge appears to be narrower and hence stronger than the eastward jet induced by the cold eddy; this is related to the asymmetry of vortex stretching.

We have seen that baroclinicity together with a localized topographic slope generates barotropic flows (or waves) as a result of JEBAR. Those barotropic waves may produce a western boundary current in a way similar to wind-forced motions described by Anderson and Gill (1975). Hence, in the context of the general ocean circulation, the JEBAR-induced barotropic flows (or waves) may contribute to the short-term variations of the western boundary current (cf. SY).

### 5.4.3 Westward motion of the baroclinic field

A simple qualitative explanation about the eddy motion over the ridge is given here in terms of vortex stretching in the lower layer.

Over the flat bottom, the planetary beta effect balances with the vortex stretching in the lower layer, which assures the westward phase propagation. [That is, for a lower-layer anticyclone (cyclone), a northward (southward) current at the eddy front compensates for the large positive (negative) vortex stretching.] The propagation speed depends on the equivalent depth  $h_1 h_2 / H$  [see (5.32)], so that a warm eddy moves faster than a cold eddy of the same size as seen in Fig. 5.6 (see also Cushman-Roisin et al., 1990). When a cold eddy (i.e., a lower-layer anticyclone) climbs the ridge, the water column in the lower layer shrinks. Since the meridional motion of the center of the baroclinic field is very weak (verified from Fig. 5.2 *a posteriori*), the resulting decrease of the positive vorticity is compensated only by the barotropic-baroclinic interaction played by the second term of (5.32). (This is also another interpretation

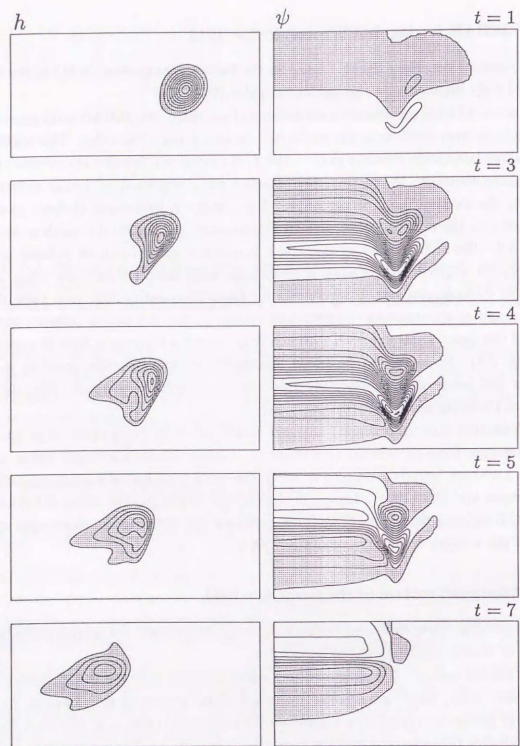


**Figure 5.2.** Evolution of the cold eddy of amplitude  $\delta = 0.2$  in the presence of the meridional ridge:  $h$  (left) and  $\psi$  (right) which are solutions to the planetary geostrophic equations. Each panel shows  $0 \leq x \leq 16$  and  $-4 \leq y \leq 4$ . The constant depth at rest has been subtracted from the values of  $h$ . Contour interval is  $5 \times 10^{-3}$  for both  $h$  and  $\psi$ . The regions of negative values are shaded.

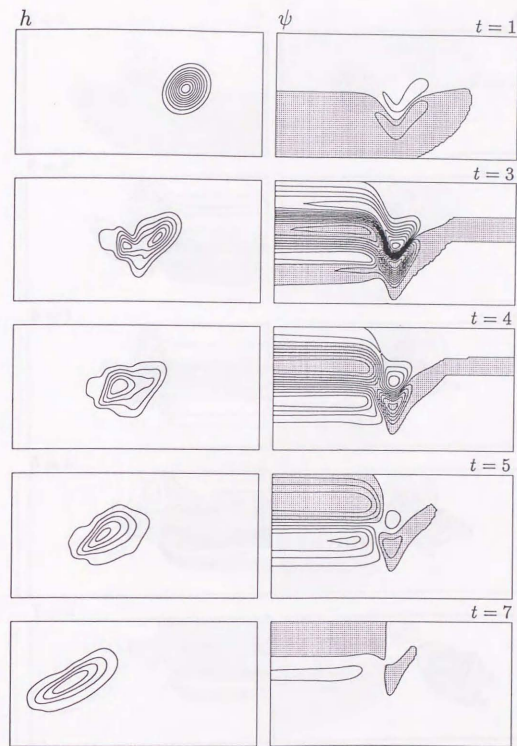


**Figure 5.3.** As in Fig. 5.2 but for the warm eddy in the presence of the meridional ridge.

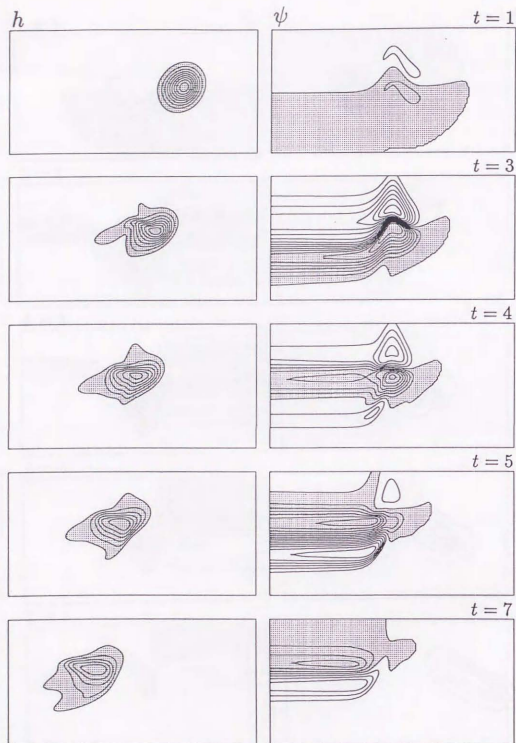


Figure 5.4. As in Fig. 5.2 but for the cold eddy in the presence of the meridional trench.

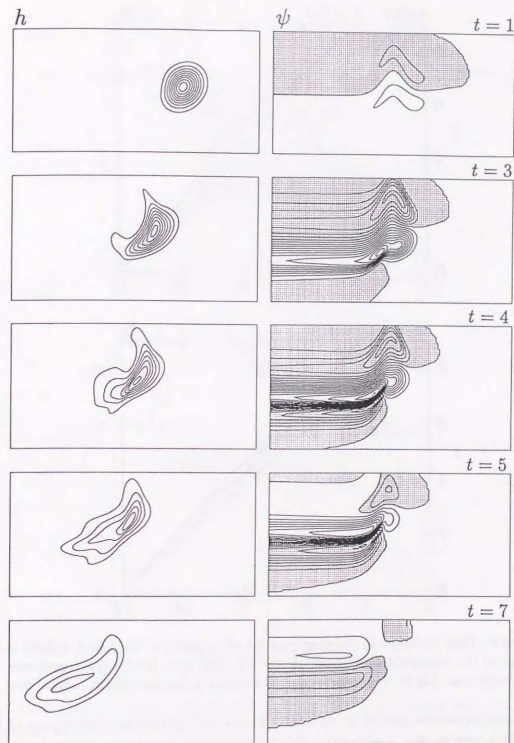
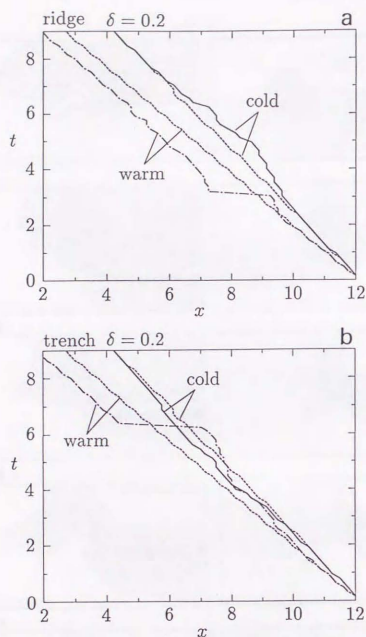


Figure 5.5. As in Fig. 5.2 but for the warm eddy in the presence of the meridional trench.



**Figure 5.6.** Time variations in the zonal position of the center of the  $h$ -field, defined as the maximum of the interface displacement. (a)  $\delta = 0.2$ , ridge case. (b)  $\delta = 0.2$ , trench case. (c)  $\delta = 0.8$ , ridge case. (d)  $\delta = 0.8$ , trench case. The dotted lines show the flat-bottom case.

of deep compensation caused by JEBAR.) That is, the horizontal convergence of the eastward barotropic flow pushing the eddy front from the west may maintain the vortex stretching (see right panels of Fig. 5.2). In other words, the westward propagation is characterized by the *effective* beta  $\beta_{\text{eff}}$  defined by

$$\beta_{\text{eff}} = \beta_0 + \frac{f^2}{g'h_1 h_2} \psi_y \quad (5.40)$$

when taking into account the JEBAR-induced flow; the above process is interpreted as  $\beta_{\text{eff}}$  reduced over the ridge. As a result, the westward propagation speed of the  $h$ -field

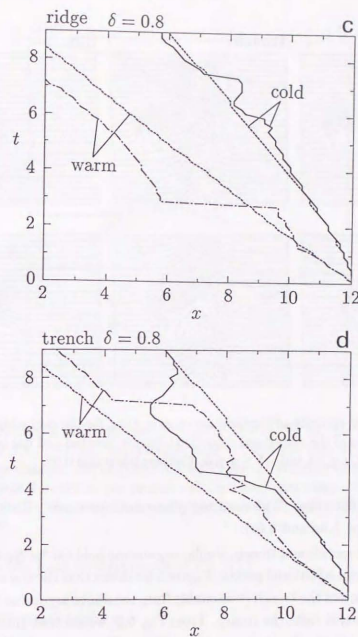


**Figure 5.6.** (Continued.)

is decreased over the ridge (left panels of Fig. 5.2; Fig. 5.6a). This is why the  $h$ -field of the eddy is steepened in the rear.

On the other hand, when a warm eddy (i.e., a lower-layer cyclone) ascends the ridge, the water column is compressed. The gain of the negative vorticity requires horizontal divergence of the westward barotropic flow advecting the eddy front westward. This process is also interpreted as the increased effective beta  $\beta_{\text{eff}}$ . Accordingly, the westward propagation of the baroclinic field is increased in the presence of the ridge (see Fig. 5.3 and 5.6a). The above qualitative explanation is confirmed by Figs. 5.6a and 5.6c. The warm eddy appears to be accelerated over the ridge, while the cold eddy appears to

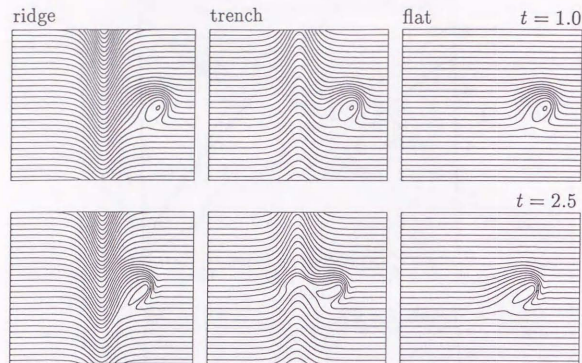


Figure 5.7. Potential vorticity of the lower layer,  $q_2 = f/h_2$ , for the cold eddy of amplitude  $\delta = 0.8$  in the presence of the meridional ridge (left), trench (middle) and flat bottom (right). Each panel shows  $2 \leq x \leq 14$  and  $-5 \leq y \leq 5$ . Contour interval is 0.05.

be decelerated over the ridge. The resulting phase shift increases with increasing the amplitude  $\delta$  (cf. Figs. 5.6a and 5.6c).

In the case of the meridional trench, similar arguments hold except for signs. Therefore, we only note some additional points. Figure 5.6b shows that the warm eddy, which is retarded when it enters the trench (reasonable from the above argument), experiences rapid translation when it exits the trench. From Fig. 5.5, we see that this is due to the strong westward barotropic flow generated by JEBAR. The western half of the trench is equivalent to the eastern flank of the ridge in this regard. Considering the property of the JEBAR forcing, the initial effect of the ridge on the westward translation has nothing to do with the downstream shape of the topography. Consequently, a bottom slope shallower to the west (e.g., the eastern flank of a meridional ridge or a western continental slope) behaves as an attractor to a warm eddy but as a repeller to a cold eddy. Grimshaw et al. (1994b) found the retardation of the westward migration of cyclonic eddies over a slope, which is consistent with the present results.

A simple insight into topography with respect to the westward motion may be possible using a map of geostrophic contours of the lower layer,  $q_2 = f/h_2$  (Fig. 5.7). The ridge (trench) appears as a band of high (low) potential vorticity. Then, for a cold eddy, the ridge acts as an obstacle (left panels of Fig. 5.7), while the trench appears to

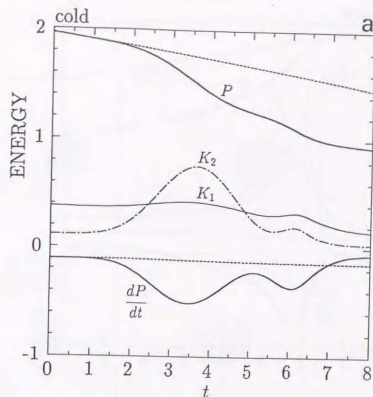


Figure 5.8. Available potential energy  $P$  (unit:  $1 \times 10^{-3}$ ), kinetic energy of the upper and lower layer ( $K_1$  and  $K_2$ , respectively; unit: 1) and the rate at which the available potential energy changes,  $dP/dt$  (unit:  $5 \times 10^{-3}$ ) for (a) the cold eddy and (b) the warm eddy of amplitude  $\delta = 0.2$  in the presence of the meridional ridge. The values of energy are area-integrated. The dotted lines added to lines for  $P$  and  $dP/dt$  correspond to the flat-bottom case.

"roll up" the eddy front (middle panels of Fig. 5.7).

#### 5.4.4 Energy conversion

When the barotropic flow is generated by the JEBAR forcing, the baroclinic field must be attenuated energetically by releasing the available potential energy. Fig. 5.8 shows this process for both cyclone (Fig. 5.8a) and anticyclone (Fig. 5.8b) propagating over the ridge. We note that the effective damping time is found to be much longer than  $\tau^{-1} = 154$  days; this is because we only assumed the damping term in the momentum equations. The rapid decrease of the available potential energy over a limited period is due to the emission of the barotropic waves above the varying bottom topography. The converted kinetic energy decreases rapidly by both transmission through the unbounded western boundary and frictional dissipation. The emission is intense when the eddy exits as well as enters the ridge, as shown in Fig. 5.8a, and relatively weak when it reaches the crest of the ridge. This is simply because the JEBAR forcing is strong at the location where the gradient of the bottom slope is large. The duration of the

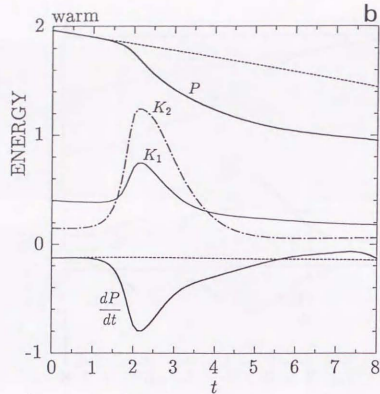


Figure 5.8. (Continued.)

energy conversion is different between cold and warm eddies in accordance with the period during which the baroclinic field passes the ridge, which is consistent with the direction of the JEBAR-induced barotropic flows transporting the baroclinic field.

The present feature in the energy conversion resembles that of baroclinic instability (e.g., Chassignet and Cushman-Roisin, 1991). However, in the present case, the barotropic and baroclinic modes are coupled only with a catalyst of sloping bottom topography.

### 5.5 JEBAR on the quasigeostrophic motion

Baroclinic eddies of radius 100–200 km are ubiquitous in the world ocean; e.g., the “MODE” eddies in the Sargasso Sea (Freeland et al., 1975) and the Loop Current in the western Gulf of Mexico [see the review in Smith (1986)]. They appear to be governed by the quasigeostrophic dynamics. We confirm the properties of JEBAR in the case of such smaller-scale motions using the quasigeostrophic equations (5.34) and (5.35).

Consider a baroclinic eddy of radius  $L = 120$  km and the other ambient parameters are the same as (5.36). Then, we have  $\beta = 0.02$ ,  $Ro = 4.2 \times 10^{-3}$  and  $\bar{F} = 9.6$ ; which satisfy the parameter regime (5.33) quite well. The baroclinic Rossby radius  $\bar{L}_D$  is 38.7 km in the present section. We take  $B = 1.0$  and  $F = 4.0$  in (5.35); the latter value

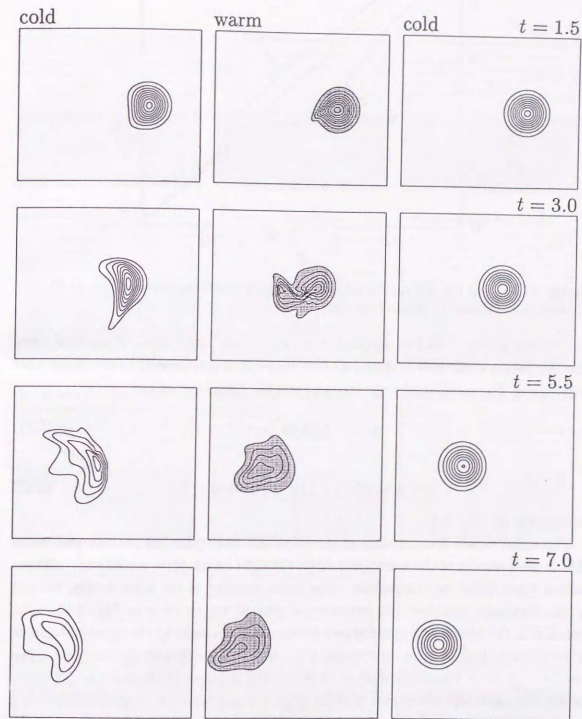
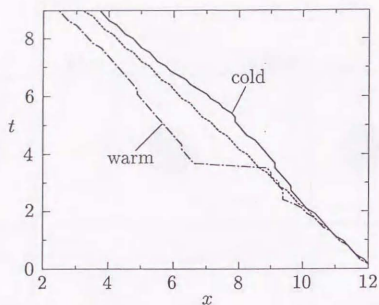


Figure 5.9. Evolution of  $\eta$  in the presence of the meridional ridge: the cold eddy (left) and the warm eddy (middle). The right panels show the solutions for the cold eddy but without topography. Each panel shows  $2 \leq x \leq 14$  and  $-5 \leq y \leq 5$ . Contour interval is 0.1. The regions of negative values are shaded.



**Figure 5.10.** As in Fig. 5.6 but for the quasigeostrophic motions corresponding to Fig. 5.9. The dotted line shows the flat-bottom case.

may be marginally valid but adopted to obtain a clear illustration of material lines. The dissipation coefficient is chosen as  $K = 0.01$  which corresponds to the decay time of 579 days. The meridional ridge (trench) and the initial values are

$$\eta_B = \pm 1.5 \operatorname{sech}^2(x - 8) \quad (5.41)$$

and

$$\eta = \pm \exp[-(x - 12)^2 - y^2] \quad \text{at } t = 0, \quad (5.42)$$

respectively (cf. Fig. 5.1).

Figure 5.9 shows the evolution of the baroclinic field  $\eta$  for both a cold and warm eddy in the presence of the meridional ridge; the right panels show a cold eddy without bottom topography for comparison. The zonal position of the eddy center, defined by the maximum interface displacement, is plotted versus time in Fig. 5.10. The evolution in the trench case is not shown because it is obtained by the quasigeostrophic antisymmetry; i.e.,  $x \rightarrow x$ ,  $y \rightarrow -y$ ,  $\psi \rightarrow -\psi$ ,  $\eta \rightarrow -\eta$  and  $\eta_B \rightarrow -\eta_B$ . The distributions of the barotropic field  $\psi$  are essentially the same as those in the planetary geostrophic cases and not shown here (cf. Figs. 5.2 and 5.3). The eddies suffer strong asymmetry in shape over the ridge by the JEBAR-induced barotropic flows as in the preceding section. The meridional ridge again repels the cold eddy and attracts the warm eddy (Fig. 5.10), which is consistent with the results of Smith and O'Brien (1983).

The evolution of the material lines associated with the eddy in the upper layer is shown in Fig. 5.11. Plotted are the values of  $q_1 = d_1(F\eta + By)$ . This figure is useful for examining the meridional motion from the Lagrangian viewpoint because water

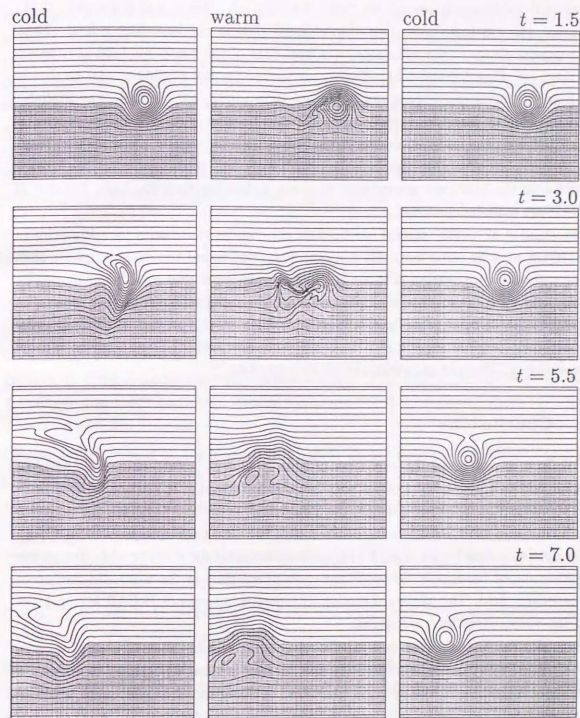


**Figure 5.11.** Potential vorticity of the upper layer,  $q_1 = d_1(F\eta + By)$ , corresponding to Fig. 5.9. Each panel shows  $2 \leq x \leq 14$  and  $-5 \leq y \leq 5$ . Contour interval is 0.1. The regions of negative values are shaded.

particles in the upper layer are frozen to the  $q_1$ -contours (e.g., McIntyre and Palmer, 1983; Davey and Killworth, 1984). It appears that the cyclone (anticyclone) drifts northward (southward) toward its "rest" latitude (cf. Davey and Killworth, 1984). However, there is little indication of meridional shift in the baroclinic  $\eta$ -field. Thus, the material center of the eddy separates from that of the baroclinic field as it passes the ridge (cf. Figs. 5.9 and 5.11). Energy conversion process is quite similar to that in the planetary geostrophic case and hence not shown here (see Fig 5.8). The available potential energy decreases rapidly when the eddy passes the ridge. This process is associated with the emission of barotropic waves with an infinite phase speed. Thus, the topographic effects on the baroclinic eddies on this particular scale are similar to those on the planetary geostrophic motions, indicating that the basic features of JEBAR are scale-independent.

Freeland et al. (1975) carried out the field experiment to measure the eddy fields in the MODE area by using neutrally buoyant floats and found the irregular phase shift in the westward propagation of those fields. They suggested that even linear baroclinic Rossby waves may reproduce such phenomena if the topographic control is taken into account. The JEBAR-propelling mechanism shown in the present experiment may support their original suggestion. In reality, however, mechanisms such as mutual induction (e.g., Flierl et al., 1980) cannot be neglected.

## 5.6 Conclusions

We have investigated the evolution of both planetary geostrophic and quasigeostrophic eddies in a two-layer ocean with bottom topography. In particular, interpreting the interaction between a single, pure baroclinic eddy and a meridional ridge (or trench) in terms of JEBAR, we have shown that the westward upslope bottom topography acts as a repeller for a cold eddy and an attractor for a warm eddy due to the JEBAR-induced barotropic flows. This causes phase shift in the westward motion of the baroclinic field. The westward motion interpreted in terms of JEBAR is consistent with the vortex-stretching argument.

It is also shown that, even without the advection terms in the governing equations, the combined effect due to baroclinicity and varying bottom topography explains the meridional migration of the eddy; a baroclinic cyclonic (anticyclonic) eddy tends to move northward (southward) with the aid of bottom topography.

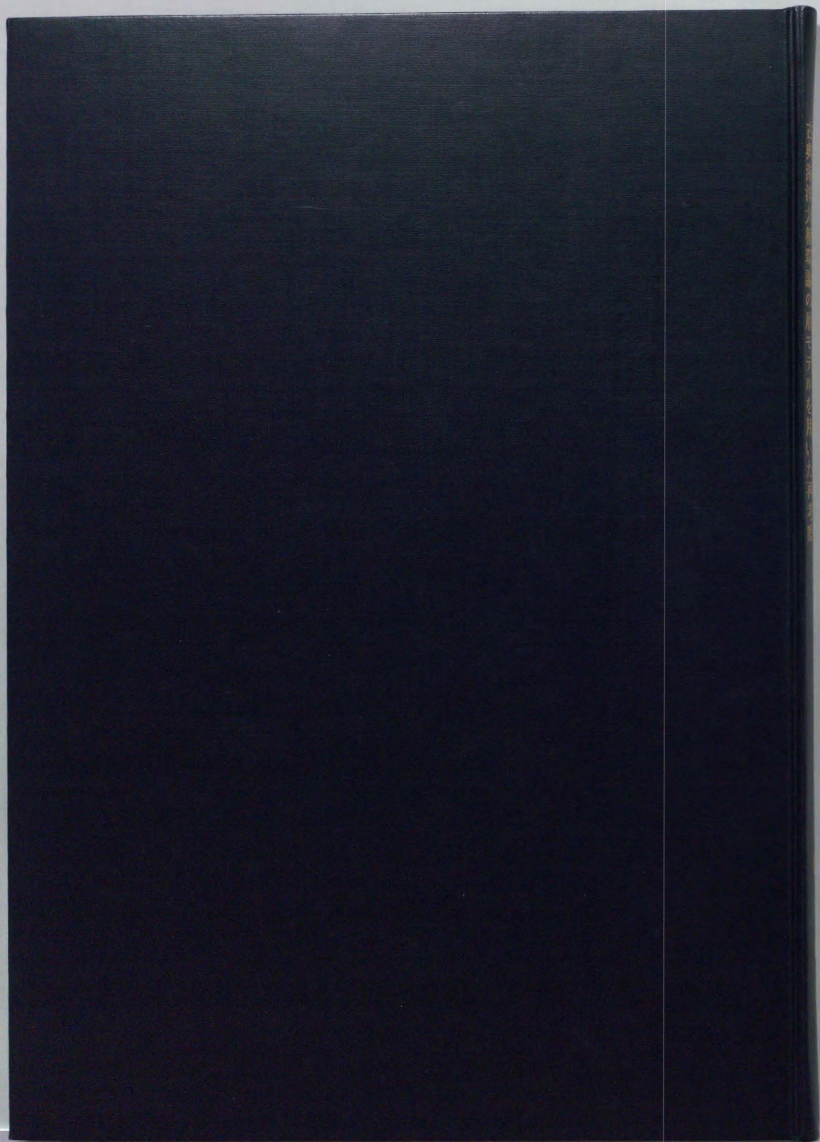
JEBAR may excite barotropic waves (or flows) wherever a baroclinic field interacts with bottom topography. Therefore, localized topography may act as a source of barotropic waves when JEBAR is in action. This situation is quite similar to sound radiation from localized turbulent flows (cf. Lighthill, 1978). We suggest that the barotropic waves thus generated may contribute to short-term variations of western

boundary currents (cf. SY). In principle, observing the barotropic wave signals near the western boundary may lead to the information of baroclinic eddies (topography) in an open ocean if the information of the topography (baroclinic eddies) is known. It is now known that the altimeter of the TOPEX/POSEIDON satellite can measure sea level with accuracy of a few centimeters (Fu et al., 1994). Despite various limitations due to model simplification, the present analysis therefore suggests one possible way to combine surface altimetry data with subsurface baroclinic fields. Actually, this mechanism which is focused on in the present article may explain qualitatively the phase speed of the baroclinic Rossby waves recently observed by the TOPEX/POSEIDON satellite altimeter (Chelton and Schlax, 1996) and the irregular excursions of the westward propagating MODE eddies (Freeland et al., 1975).

## References

- Anderson, D. L. T. and A. E. Gill. 1975. Spin up of a stratified ocean with applications to upwelling. *Deep-Sea Res.* **22**, 583-596.
- Barnier, B. 1988. A numerical study on the influence of the Mid-Atlantic Ridge on nonlinear first-mode baroclinic Rossby waves generated by seasonal winds. *J. Phys. Oceanogr.* **18**, 417-433.
- Chassignet, E. P. and B. Cushman-Roisin. 1991. On the influence of a lower layer on the propagation of nonlinear oceanic eddies. *J. Phys. Oceanogr.* **21**, 939-957.
- Chelton, D. B. and M. G. Schlax. 1996. Global observations of oceanic Rossby waves. *Science* **272**, 234-238.
- Cushman-Roisin, B., E. P. Chassignet, E. P., and B. Tang. 1990. Westward motion of mesoscale eddies. *J. Phys. Oceanogr.* **20**, 758-768.
- Davey, M. K. and P. D. Killworth. 1984. Isolated waves and eddies in a shallow water model. *J. Phys. Oceanogr.* **14**, 1047-1064.
- Flierl, G. R., V. D. Larichev, J. C. McWilliams, and G. M. Reznik. 1980. The dynamics of baroclinic and barotropic solitary eddies. *Dyn. Atmos. Oceans* **5**, 1-41.
- Freeland, H. J., P. B. Rhines, and T. Rossby. 1975. Statistical observations of the trajectories of neutrally buoyant floats in the North Atlantic. *J. Mar. Res.* **33**, 383-404.
- Fu, L.-L., E. J. Christensen, C. A. Yamarone, Jr., M. Lefebvre, Y. Ménard, M. Dorrer, and P. Escudier. 1994. TOPEX/POSEIDON mission overview. *J. Geophys. Res.* **99**, 24369-24381.

- Greatbatch, R. J., A. F. Fanning, A. D. Goulding, and S. Levitus. 1991. A diagnosis of interpentadal circulation changes in the North Atlantic. *J. Geophys. Res.* **96**, 22009–22023.
- Grimshaw, R., D. Broutman, X. He, and P. Sun. 1994a. Analytical and numerical study of a barotropic eddy on a topographic slope. *J. Phys. Oceanogr.* **24**, 1587–1607.
- Grimshaw, R., Y. Tang, and D. Broutman. 1994b. The effect of vortex stretching on the evolution of barotropic eddies over a topographic slope. *Geophys. Astrophys. Fluid Dyn.* **76**, 43–71.
- Henrotay, P. 1981. Topographic effects on solitary Rossby waves. *Dyn. Atmos. Oceans* **6**, 29–47.
- Lighthill, M. J. 1978. *Waves in Fluids*, Cambridge University Press, Cambridge.
- Louis, J. P. and P. C. Smith. 1982. The development of the barotropic radiation field of an eddy over a slope. *J. Phys. Oceanogr.* **12**, 56–73.
- McIntyre, M. E. and T. N. Palmer. 1983. Breaking planetary waves in the stratosphere. *Nature* **305** 593–600.
- McWilliams, J. C. and G. R. Flierl. 1979. On the evolution of isolated, nonlinear vortices. *J. Phys. Oceanogr.* **9**, 1155–1182.
- Myers, P. G. and A. J. Weaver. 1996. On the circulation of the North Pacific Ocean: Climatology, seasonal cycle and interpentadal variability. *Prog. Oceanogr.* in press.
- Myers, P. G., A. F. Fanning, and A. J. Weaver. 1996. JEBAR, bottom pressure torque and Gulf Stream separation. *J. Phys. Oceanogr.* **26**, 671–683.
- Sakamoto, T. and T. Yamagata. 1996. Seasonal transport variations of the wind-driven ocean circulation in a two-layer planetary geostrophic model with a continental slope. *J. Mar. Res.* **54**, 261–284.
- Salmon, R. 1992. A two-layer Gulf Stream over a continental slope. *J. Mar. Res.* **50**, 341–365.
- Smith, D. C., IV. 1986. A numerical study of Loop Current eddy interaction with topography in the western Gulf of Mexico. *J. Phys. Oceanogr.* **16**, 1260–1272.
- Smith, D. C., IV and J. J. O'Brien. 1983. The interaction of a two-layer isolated mesoscale eddy with bottom topography. *J. Phys. Oceanogr.* **13**, 1681–1697.
- Williams, G. P. and T. Yamagata. 1984. Geostrophic regimes, intermediate solitary vortices and Jovian eddies. *J. Atmos. Sci.* **41**, 453–478.



# Classical Ocean General Circulation Theory Revisited Using Layer Models

Toshihiro Sakamoto

## PART I

### DISCONTINUOUS SOLUTIONS OF TWO- LAYER PLANETARY GEOSTROPHIC EQUATIONS

#### 1. Discontinuities in the Sverdrup interior

Sverdrup dynamics is reformulated based on an inviscid/hyperbolic system of two-layer planetary geostrophic equations instead of the conventional vorticity approach. The integral conservation laws of momentum are introduced to investigate solutions which may include jump discontinuities subject only to the eastern boundary condition. An oceanic front such as a surfacing line and a closed geostrophic contour is interpreted as a "shock" across which the following jump conditions derived from these integral constraints are satisfied:

$$\left[ p \right] = \left[ h_1 - \frac{h_1^2}{2H} \right], \quad f \left[ \psi_1 \right] = \left[ \frac{h_1^2}{2} - \frac{h_1^3}{3H} \right],$$

where  $p$  is the (nondimensional) depth-independent pressure,  $h_1$  is the upper-layer thickness,  $H$  is the total depth,  $f$  is the Coriolis parameter and  $\psi_1$  is the upper-layer streamfunction. These may be used to determine suitable positions of fronts separating different dynamical regions if the interface structure for each subdomain is specified. Several examples demonstrate the applicability of this approach: Of particular interest is the finite-depth version of Parsons' model, in which case we can obtain the exact solution for the surfacing line in contrast to the asymptotic solution derived by Kamenkovich and Reznik (1972). It is also found that a surfacing line for Parsons' model, which is the limit as  $H \rightarrow \infty$ , can totally be determined provided that the wind forcing and the eastern boundary condition are prescribed. The present inviscid/hyperbolic perspective eliminates the need for the semigeostrophic condition used in similar studies by Parsons (1969), Veronis (1973) and Huang and Flierl (1987).

#### 2. The two-layer extension of the Stommel problem with outcropping: A numerical approach

A two-layer planetary geostrophic model with interfacial and bottom frictions is examined numerically. We have found a class of solutions which are

characterized by a viscous interior layer associated with outcropping. When the lower layer is very thick, Parsons-type solutions are reproduced. The numerical solutions are in gross qualitative agreement with the analytical solutions of Kamenkovich and Reznik (1972), although compensation seems to be imperfect near the western boundary even when the total depth is ten times the upper-layer thickness. When the lower layer is moderate, namely, as thick as the whole thermocline, the solutions are characterized by the ventilated circulation contained in the unventilated pool. When the lower layer is thin, the ventilated and unventilated circulations are separated between which the submerged layer is perfectly compensated. It is shown that the interface displacement between the outcrop and the pool increases as the bottom friction coefficient decreases, implying a jump discontinuity in an inviscid limit. With sufficiently strong winds, a part of the ventilated circulation cannot enter the western boundary layer to close on itself in the eastern interior. These types of solutions (the moderate and thin cases) cannot be covered by the so-called ventilated thermocline theory developed in the 1980s. This is primarily because the latter "modern" theory assumes the tight thermal interaction between the ocean and the atmosphere implicitly; the gyre cannot be closed near the western coast. We also suggest that the inviscid models for the ventilated thermocline may be developed further by taking into account jump discontinuities.

#### Appendix to Chapter 2. Numerical solution to Parsons' model using TVD schemes

Various TVD schemes are applied to a 1.5-layer planetary geostrophic model and are successful in representing the outcropping lower layer numerically. Two preliminary experiments concerning the evolution of a conceptual planetary eddy and the spin-up of an equatorial ocean confirm that Yee's (both symmetric and upwind) schemes capture the propagation of a baroclinic long Rossby wave reasonably well. It is also verified that the symmetric scheme is slightly more diffusive than the upwind scheme. These TVD schemes can reproduce a subtropical gyre with interior jets; the numerical solutions are in good qualitative agreement with

Parsons' analytical solution. However, the upwind scheme creates a spurious overshooting of the western boundary current when a coarse grid is used, as has been met by the previous workers using the FCT algorithm. The numerical solutions with sufficiently fine grids show that the western boundary layer separates at a higher latitude compared with the analytical solution. This disagreement suggests that the simple composition of the western boundary layer and interior layer, as performed by Parsons (1969), does not provide the correct boundary layer separation.

## PART II

### OTHER PROBLEMS

#### 3. Potential vorticity homogenization in a two-layer wind-driven gyre

A wind-driven subtropical gyre with a frictional western boundary current is investigated using a two-layer quasigeostrophic model without the advection of relative vorticity. It is shown that homogenization of the lower-layer potential vorticity  $q_2$  occurs when the zonal advective motion is so retarded by the baroclinic long Rossby wave that information on  $q_2$  cannot propagate eastward from the western boundary layer. The southward Sverdrup flow simply advects  $q_2$ -contours to leave a gap which should be filled with uniform potential vorticity if the direct vorticity input by the source term remains small. These requirements may be satisfied provided that

$$F_2 < \frac{2}{\pi}, \quad F_2 b_2 \ll \frac{1}{\pi^2},$$

where  $F_2 = F/\alpha$ ,  $b_2 = \delta/\alpha$  ( $F$ : the baroclinic rotational Froude number,  $\delta$ : the bottom friction coefficient,  $\alpha$ : the ratio of the mean lower- to upper-layer thickness). It is confirmed that this prediction agrees well with the numerical results. It is also found that this condition is consistent with the structure of the viscous western boundary layer: When  $F_2 \gg 1$ , the boundary layer for  $q_2$  is closely related to the heat equation and has the width  $O(F_2^{-1/2} \delta)$ . Since it is narrower than the boundary current of width  $O(\delta)$ , the interior distribution of  $q_2$  is strongly affected by the boundary current. When  $F_2$  satisfies the above inequalities, however, the  $q_2$ -layer becomes wider than the boundary current, so that the uniform distribution of  $q_2$  in the interior may be matched with the boundary values.

#### 4. Gyres induced by curl-free winds in the tropics

A 2.5-layer model is examined to provide a mechanism which can generate steady equatorial gyres

without nonlinearity even if zonal winds have no curl. Steady divergent flows directly driven by the zonal winds with the aid of diapycnal density mixing produce vortex stretching which appears as an external forcing in a vorticity equation to induce rotational barotropic flows in each layer. This process always leads to rotational stacked gyres however small the mixing coefficients may be. This mechanism may be applied dramatically to possible barotropic circulations in the tropics. For easterly winds, a 2.5-layer representation is a reasonable approximation for the equatorial ocean because of the equatorial upwelling. In this case, the vertically integrated transport may be cyclonic if the density mixing in the middle layer is so strong that the undercurrent overwhelms the surface jet. For westerly winds, on the other hand, the Ekman downwelling allows to use a 1.5-layer model as a better simplification for the equatorial ocean, and hence the cyclonic gyres are naturally obtained. In this way, we expect a pair of cyclonic barotropic gyres straddling the equator regardless of the zonal wind direction. This surprising property is actually observed in the several OGCM results (e.g., Semtner and Holland, 1980; Philander and Pacanowski, 1980; Liu et al., 1994). We suggest, therefore, that diapycnal density mixing is one way to extract cyclonic vorticity from the rotating solid earth which establishes a suitable density stratification in accordance with the direction of zonal winds.

#### 5. The concept of JEBAR: Evolution of baroclinic planetary eddies over localized bottom topography

The concept of JEBAR and its advantage are demonstrated in terms of a time-dependent problem concerning more idealistic situations, because JEBAR still causes a lot of misleading understandings. Numerical experiments have been conducted to investigate the evolution of pure baroclinic eddies using two-layer planetary geostrophic equations in the presence of localized bottom topography. It is shown that the emission of barotropic flows (or waves), westward acceleration and energy conversion occur when an eddy interacts with bottom topography. A meridional ridge acts as a repeller for a cold eddy and an attractor for a warm eddy due to JEBAR-induced barotropic flows (or waves), which is consistent with the vorticity argument. This mechanism may provide a possible explanation not only for the global distribution of the phase speed of baroclinic Rossby waves observed in the Pacific by the TOPEX/POSEIDON satellite altimeter but also for the abrupt change in the trajectories of the westward propagating baroclinic eddies observed in the North Atlantic.